THE JOURNAL OF PHYSICAL CHEMISTRY C

Article

Cite This: J. Phys. Chem. C 2018, 122, 7525−7532

pubs.acs.org/JPCC

Optomechanical Thermometry of Nanoribbon Cantilevers

Anupum Pant,[†,⊥] Bennett E. Smith,[‡,⊥] Matthew J. Crane,[§] Xuezhe Zhou,[†] Matthew B. Lim,[†] Stuart A. Frazier,[†] E. James Davis,[§] and Peter J. Pauzauskie*[,†,∥]

[†]Materials Science and Engineering Department, University of Washington, Seattle, Washington 98195-2120, United States

[‡]Chemistry Department, University of Washington, Seattle, Washington 98195-2120, United States

[§]Chemical Engineering Department, University of Washington, Seattle, Washington 98195-2120, United States

[∥]Physical & Computational Sciences Directorate, Pacific Northwest National Laboratory, Richland, Washington 99352, United States

Supporting Information

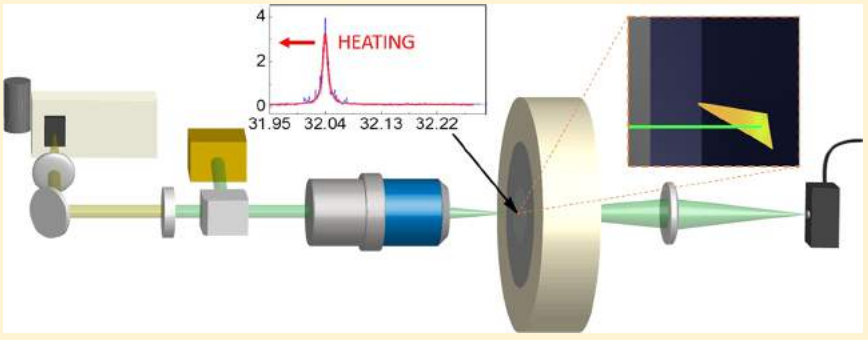

ABSTRACT: Cadmium sulfide (CdS) nanostructures have attracted a significant amount of attention for a variety of optoelectronic applications including photovoltaic cells, semiconductor lasers, and solid-state laser refrigeration due to their direct bandgap around 2.42 eV and high radiative quantum efficiency. Nanoribbons (NRs) of CdS have been claimed to laser cool following excitation at 514 and 532 nm wavelengths by the annihilation of optical phonons during anti-Stokes photoluminescence. To explore this claim, we demonstrate a novel optomechanical experimental technique for microthermometry of a CdSNR cantilever using Young's modulus as the primary temperature-dependent observable. Measurements of the cantilever's fundamental acoustic eigenfrequency at low laser powers showed a red-shift in the eigenfrequency with increasing power, suggesting net heating. At high laser powers, a decrease in the rate of red-shift of the eigenfrequency is explained using Euler−Bernoulli elastic beam theory, considering Hookean optical-trapping force. A predicted imaginary refractive index for CdSNR based on experimental temperature measurement agrees well with a heat transfer analysis that predicts the temperature distribution within the cantilever and the time required to reach steady state (<100 μs). This approach is useful for investigating solid-state laser refrigeration of a wide variety of material systems without the need for complex pump/probe spectroscopy.

INTRODUCTION

Cadmium sulfide nanostructures have been investigated for a number of applications including optically pumped nanolasers,[1,2] photocatalysis,[3,4] and, more recently, solid-state laser refrigeration[5] due to the material's direct optical bandgap,[6] large electron/phonon (Frölich) interaction,[7] and high external radiative quantum efficiency.[5] A number of stringent material properties are required for solid-state laser cooling of semiconductors to occur, including high optical absorption, low nonradiative relaxation rates, significant Huang−Rhys factors, and near-unity external radiative quantum efficiency.[8,9] Zhang et al. reported that nanoribbons of CdS could be laser cooled by as much as 40 K below room temperature using continuous-wave optical pumping at wavelengths λ = 514.5 and 532 nm.[5] It was also claimed that the thickness of the CdS material must be between 60 and 120 nm.[10] If the thickness was too small, nonradiative recombination at surfaces was hypothesized to reduce the external radiative quantum efficiency below the fundamental thermodynamic constraint for laser cooling to occur (~98%). If the thickness was greater than 120 nm, the high index of refraction of CdS nanoribbons was predicted to produce a significant amount of total internal reflection and subsequent reabsorption within the cantilever, resulting in heating.

Making direct thermal measurements of materials during laser refrigeration experiments is challenging given that direct physical contact with thermocouples can conduct heat, limiting the minimum achievable temperatures.[11] Noncontact optical thermometry methods, including ratiometric themometry,[12−14] differential luminescence thermometry,[15] and dynamic forward

Received: January 11, 2018
Revised: March 10, 2018
Published: March 12, 2018

DOI: 10.1021/acs.jpcc.8b00365
J. Phys. Chem. C 2018, 122, 7525−7532

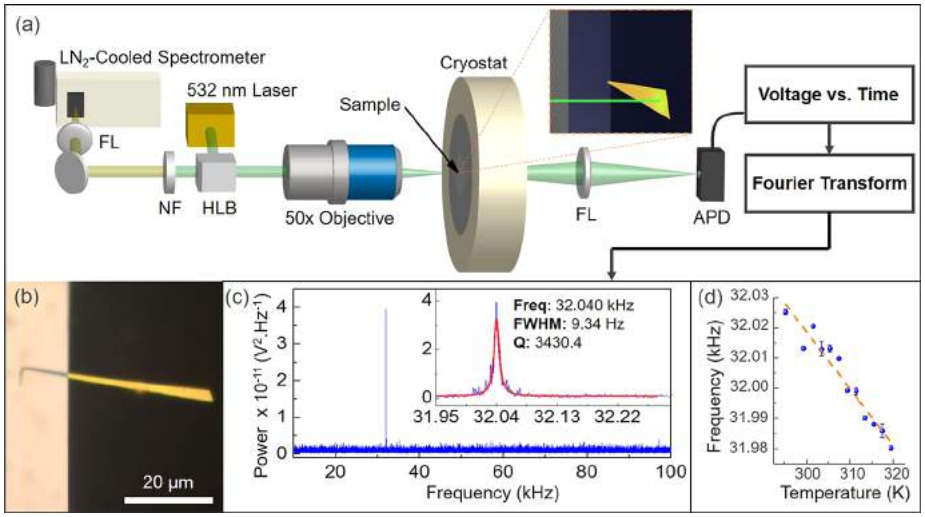

Figure 1. (a) Schematic of the experimental setup for the eigenfrequency measurement of a CdS cantilever at the edge of a silicon chip, mounted in a cryostat under vacuum. A 532 nm laser was used as the probe, focused on to the tip of the cantilever using a 50× long working distance objective lens to a spot radius of 1.15 μm. The forward-scattered light was focused onto the avalanche photodiode (APD) detector, and the resultant voltage vs time is Fourier transformed to obtain the cantilever's eigenfrequency. Backscattered light was focused onto a liquid nitrogen (LN_2) cooled spectrometer to record the PL and Raman spectra. FL, HLB, and NF stand for focusing lens, holographic beam splitter cube, and notch filter, respectively. (b) A bright-field optical image of one cantilever resting on a silicon chip (left side) and suspended over free-space (right side). (c) The Fourier-transformed signal shows a lone sharp Lorentzian peak centered at 32.040 kHz. The inset shows a magnified x-axis of the same data and a fitted Lorentzian curve in red. (d) A frequency vs temperature calibration of data points is shown in blue circles, and a linear least-squares fit of the data is shown with an orange dotted line.

light scattering[12] avoid this pitfall and allow the laser to simultaneously cool and measure the local temperature. However, these methods require irradiance-dependent calibrations. Also, pumping electronic states to induce cooling can modify their energies and requires careful considerations to decouple the incident irradiance from cooling measurements.[13] A pump−probe luminescence thermometry (PPLT) approach was used by Zhang et al.[5] to explore CdS laser refrigeration. In this method, a cooling laser at either 514 or 532 nm pumped the sample to generate anti-Stokes photoluminescence (PL), and a subsequent probe laser at 473 nm was used to excite temperature-dependent band-edge PL, which was used to measure the temperature via a Varshni calibration.[5] Time constants on the order of several minutes were observed for the sample to warm back to room temperature after the cooling laser was turned off. This same method was used to claim laser cooling of perovskites.[16] One challenge in interpreting photoluminescence data is that band-edge energies are also dependent on the carrier excitation density.[17] This motivates a need for experimental optical thermometry methods that are noncontact and independent of excited carrier densities.

In this work, we present an optomechanical method for measuring the temperature of suspended CdS nanoribbon cantilevers by observing the fundamental acoustic eigenfrequency of the cantilever using forward-scattered continuous-wave laser interferometry, analogous to the softening of breathing modes with increasing laser powers[18] measured by ultrafast time-resolved studies[19] in metal nanostructures. A modified Euler−Bernoulli beam model was used to interpret the data by accounting for temperature-dependent changes in the material's Young's modulus and optical dipole-trapping forces[20] that act on the suspended cantilever.

EXPERIMENTAL DETAILS

The cadmium sulfide nanoribbons (CdSNR) were synthesized using a chemical vapor transport (CVT) process conducted in a programmable tube furnace (Lindberg Blue M). Cadmium sulfide powder (650 mg, 99.995% Sigma-Aldrich) in an alumina boat was used as the source and placed at the center of the tube furnace. The growth substrates were prepared by dropping a dilute gold nanocrystal (AuNC, 30 nm) solution in chloroform on a silicon (100) surface. The substrates were left to rest for a few minutes to allow the solvent to evaporate and then were transferred onto a quartz tray. The quartz tray was loaded into a tube furnace such that the silicon substrates were downstream 7−10 cm inside the edge of the furnace. Argon + 5% H_2 was used to initially flush the chamber for 30 min at 400 SCCM. The flow rate was then reduced to 50 SCCM, and the temperature was ramped up to the growth temperature (T_g) in 30 min. The growth temperature was maintained for the growth time (t_g), and the furnace was allowed to cool naturally.

Dry transfer of as-grown CdSNRs was conducted by gently inverting a cleaved silicon wafer onto the as-grown substrate. Individual CdSNRs were then removed from the transfer substrate and placed at the edge of another clean silicon substrate to form a cantilever (as shown in Figure 1b) using a nanomanipulator (Märzhäuser-Wetzlär) with a tungsten dissecting probe (World Precision Instruments) with a sufficiently small tip radius-of-curvature (~100 nm).

The silicon substrate loaded with the CdSNR cantilever sample was then attached via a copper tape to the stage of an optical cryostat (Janis ST-500) that was modified by drilling a hole down its center line. Cantilevers were suspended over the stage's axial hole to allow forward-scattered laser radiation to be collected from behind the chamber (Figure 1a,b). The chamber was pumped down to a pressure of 4.0×10^{-4} mbar using an oil-free turbo molecular pump. The cryostat stage was then aligned into an optical setup to measure the cantilever's

DOI: 10.1021/acs.jpcc.8b00365
J. Phys. Chem. C 2018, 122, 7525−7532

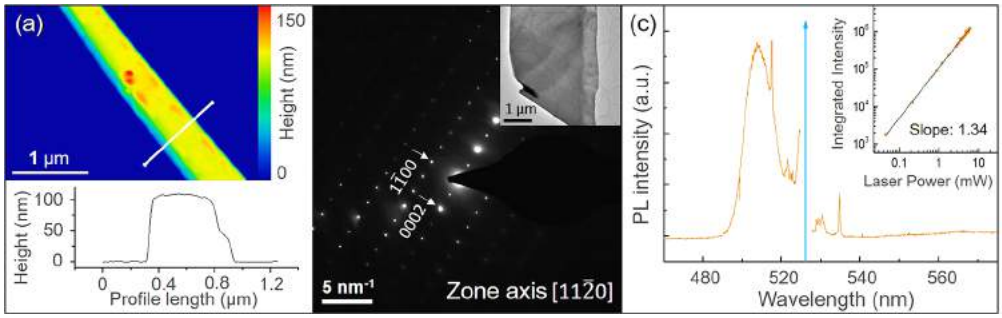

Figure 2. (a) AFM scan of the NR surface resting on silicon, with a white profile line straddling across the NR width (top). The corresponding line profile is shown below, revealing a 110 nm thickness. (b) A select area electron diffraction pattern of the NR shown in the inset. (c) A room temperature PL spectrum collected from the suspended part of the cantilever, measured using an incident 532 nm laser with 2 kW/cm^2 irradiance. The inset shows a corresponding log−log plot of the integrated PL intensity as a function of the laser power.

eigenfrequency. A single-longitudinal-mode 532 nm laser beam (Coherent, Compass 532) was first split using a holographic transmission grating and focused on the tip of the cantilever using a 50× long working distance objective lens (Mitutoyo). The transmitted light was focused on a high-speed avalanche photodiode (APD, Thorlabs APD430A). The voltage versus time signal obtained from APD over 1 s was then Fourier transformed using a LabVIEW program to obtain one power spectrum. Thirty power spectra were averaged to obtain one measurement, as shown in the Figure 1c. The peak then was fit to a Lorentzian shape to obtain the cantilever's eigenfrequency. An average frequency data point was obtained by fitting six measurements obtained at the same laser power with a gap of 1 min between consecutive measurements. The error bars represent one standard deviation. Temperature calibration was performed by heating the cryostat using a temperature controller (Lake Shore 335, resolution: 10 mK), and measuring the eigenfrequency of the cantilever at different temperatures using a low laser irradiance (5 kW/cm^2) that does not measurably heat the sample. An average frequency data point was obtained by fitting three measurements obtained at the same temperature with a gap of 1 min between consecutive measurements. The error bars represent one standard deviation.

RESULTS AND DISCUSSION

Following synthesis, the silicon substrates were observed to be coated with a brightly yellow colored layer of densely packed CdSNRs. The general shape of a single nanoribbon exhibited either a tapered wedge shape or a rectangular ribbon morphology, suggesting a combined vapor−liquid−solid (VLS) and vapor−solid (VS) growth mechanism.[21−23] The typical height (thickness) and widths of the NRs were 50−250 nm and 1−5 μm, respectively. However, NRs with thicknesses in the range 50−120 nm were used for our experiments following prior claims of thickness-dependent laser refrigeration.[10]

As a result of variation in the growth parameters, the NR morphologies were observed to decrease in height and increase in width as T_g was increased from 780 to 840 °C, and increase in length as t_g was increased from 30 min to 4 h. For our experiments, a T_g = 840 °C and a t_g = 4 h were selected to produce thin, long, and wide NRs, within the height range 65−120 nm[10] desirable for laser cooling and to maximize the area of the laser spot incident on the NR. Preliminary external quantum efficiency (EQE) measurements based on all-optical scanning laser calorimetry (ASLC)[24] showed EQE values ranging from 0.7735 to 0.9899. Although the measured EQE values appear to be lower than the required threshold for obtaining laser cooling, the laser radiation of 440−480 nm used to conduct these measurements was observed to induce photodamage in the CdSNRs. In one such case, EQE values were measured as near unity before photodamage, which dropped to 0.8 after the photodamage was inflicted. These measurements will be presented in greater detail in an upcoming paper.

Eigenfrequency measurements as described in the previous section were made on a representative CdSNR cantilever sample with an NR length, width, and height of 45.6 μm, 2.3 μm, and 110 nm, respectively. The length of the suspended part of the cantilever was 35 μm. A Fourier transformation of the APD signal produced a thermomechanical noise spectrum,[25,26] with a major peak from the cantilever's fundamental bending mode (Figure 1c). Using standard Lorentzian peak fitting, an eigenfrequency f_0 = 32 040 Hz, an fwhm (Δf_0) of 9.34 Hz, and a high quality factor ($Q = f_0/\Delta f_0$) of 3430.4 were measured at room temperature and 4.0 × 10^{-4} mbar pressure, and with a laser irradiance of ∼1.0 kW/cm^2 (Figure 1c, inset). A temperature calibration was done at a low laser irradiance (5 kW/cm^2), by measuring the eigenfrequency of the cantilever while heating the cryostat in steps of 2 K from 295 to 320 K. At this low irradiance, the frequency versus temperature data displayed in Figure 1d show a linear red-shift of the eigenfrequency with increasing temperature yielding a slope of −1.89 Hz/K. This corresponds to an overall measured decrease in the eigenfrequency of 37.8 Hz. This frequency shift corresponds to an internal temperature increase (ΔT_{ms}) of approximately 20.6 K when using the isothermal cryostat calibration discussed above. However, at high laser irradiances a temperature gradient is established in the cantilever, and numerical calculations must be made to correlate how measured eigenfrequency values at isothermal conditions correlate to eigenfrequencies that exist in the context of a temperature gradient. According to finite element (COMSOL[27]) simulations of a nonisothermal cantilever with a spatially varying Young's modulus (Figure S10), the measured temperatures (ΔT_{ms}) are a close representation of a laser heated CdSNR cantilever with a $\Delta T_{max} \approx 4.03 \times \Delta T_{ms}$ (see SI for details).

An AFM scan (Figure 2a) of the cantilever surface resting on the silicon wafer demonstrates that the surface of the cantilever is flat with a thickness of 110 nm, and a surface RMS roughness <1 nm. Consistent with extensive TEM diffraction studies on isomorphic ZnTe NRs,[28] TEM select area electron diffraction

DOI: 10.1021/acs.jpcc.8b00365
J. Phys. Chem. C 2018, 122, 7525−7532

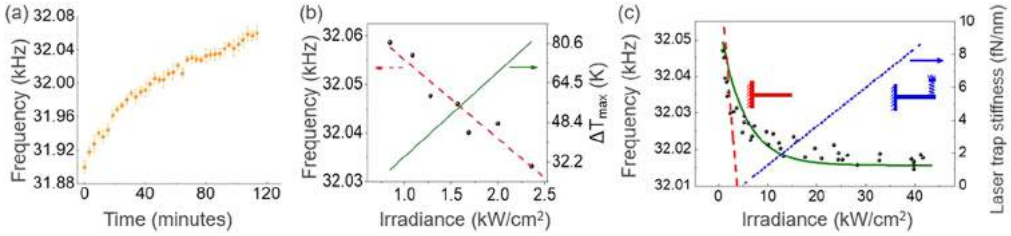

Figure 3. (a) Blue-shift and eventual saturation of the eigenfrequency observed when measurements were done immediately after loading the cantilever sample into the cryostat, with a 11.5 kW/cm^2 laser irradiance for a span of 2 h. (b) Eigenfrequency measurement at low laser irradiances (below 2.5 kW/cm^2) shows a linear red-shift of eigenfrequency with increasing laser irradiance. A least-squares linear fit is shown using a red dotted line. On the basis of the temperature calibration, a green line shows the variation of the ΔT_{max} on the right vertical axis. (c) Eigenfrequency measurement data points shown as black dots on the cantilever taken at random laser irradiances to account for hysteresis. The data fit to an exponential decay curve shown in solid green line. Young's-modulus-dependent frequency shift component which is dominant at low laser irradiances has been shown using a dashed red line, while at higher irradiances the laser-trapping stiffness component obtained by subtracting the heating component from the exponential fit has been shown as a dotted blue line. The laser trap stiffness values estimated using theory (Figure S4a,b) have been shown in the right vertical axis.

(SAED) (Figure 2b) of the CdSNR shows a single crystal wurtzite diffraction pattern from the $[11\bar{2}0]$ zone axis of a representative NR sample, with the planes $[1\bar{1}00]$ and [0002] marked. A room temperature photoluminescence spectrum collected from the suspended part of a representative cantilever sample (Figure 2c) using a 532 nm excitation source shows a typical band-to-band anti-Stokes PL curve centered at 510 nm, matching the spectra reported by Zhang et al.[5] Recently reported time-resolved measurements indicate that the anti-Stokes luminescence is produced from optical transitions between real states.[29] Peaks in the PL at 299 and 600 cm^{-1} correspond to the 1LO and 2LO phonon modes, confirming the high crystallinity of CdSNRs. The red-shift in the 1LO mode in our measurements compared to the reported Raman modes for a single crystal of bulk CdS[30] at 305 and 600 cm^{-1} can be attributed to the phonon confinement effect in the nanostructure.[31−33] The peaks at 204 and 245 cm^{-1} stem from the surface reconstruction of the CdSNR.[34] The inset of Figure 2c shows an integrated PL intensity with laser power, depicting no apparent saturation of intensity at laser powers as high as 8 mW or an irradiance of 192.4 kW/cm^2. We note that although some cantilever structures were observed to withstand high-power laser irradiation as mentioned above, most cantilevers decomposed at irradiances as low as 72 kW/cm^2. This discrepancy may arise from local variations in the material's absorption coefficient, or morphology-dependent resonances (MDRs)[35,36] which can cause a peak in absorption for certain thicknesses near 102 nm (Figure S1). To avoid any permanent damage to the samples during the eigenfrequency experiments, laser irradiances were kept under 43.3 kW/cm^2, corresponding to a total laser power of 1.8 mW in a spot diameter of 2.3 μm.

An interesting blue-shift of eigenfrequency was observed immediately after loading the sample into the cryostat. A representative sample was loaded, and the eigenfrequency was continually recorded with a laser beam irradiance of 11.5 kW/cm^2 over a period of 2 h, during which it shifted from 31 900 Hz to a steady state value of 32 060 Hz (Figure 3a). Upon switching off the laser overnight and repeating the measurement, the eigenfrequency remained stable within standard deviations of a higher steady state value around 32 020 Hz over 40 min (Figure S9). All of the eigenfrequency measurements discussed below were conducted after irradiation of the cantilever tip for 2 h when the eigenfrequency reached a steady state value. The blue-shift suggests that the laser induces an irreversible modification of the mass distribution of the cantilever around the incident laser spot area and reaches a steady state. Although a blue-shifting frequency trend could be attributed to the cooling of the cantilever structure, the observed irreversible change in the eigenfrequency is inconsistent with this laser-cooling hypothesis. Surface adsorbates may desorb upon irradiation, decreasing the cantilever's local linear mass density, and leading to a blue-shift in the measured eigenfrequency.

The data in Figure 3b,c were acquired at random laser irradiances to account for potential hysteresis effects or irreversible desorption of foreign species. Figure 3b demonstrates a red-shift in eigenfrequency with an increasing laser irradiance in the low laser irradiance range (<2.5 kW/cm^2). A least-squares linear fit to the data is shown using a red-dotted line. The y-axis intercept of the linear fit was used to obtain the first natural resonant frequency mode ("diving board mode") of the cantilever of 32 071 Hz at room temperature in the absence of laser perturbation. The decrease in eigenfrequency in the low irradiance range can be attributed to a decrease in the Young's modulus of the material as the cantilever heats up with an increase in laser irradiance. The magnitude of the measured increase at the hottest point within the cantilever (ΔT_{max}) was estimated using the aforementioned temperature calibration as shown using a green line in the right y-axis. Using this, a ΔT_{ms} (ΔT_{max}) of 20.6 K (82.4 K) above room temperature at a laser irradiance of 2.5 kW/cm^2 was determined. Temperature measurements made on CdSNRs from Zhang et al.,[5] using the same method, also suggested heating (Figure S8).

Using COMSOL[27] finite element analysis, the geometry of the cantilever was modeled, and the first eigenfrequency mode (Figure S2) was probed by varying the Young's modulus from 44 to 46 GPa. A linear increase of eigenfrequency from 32 831 to 33 569 Hz with increasing Young's modulus (slope: 368.9 Hz/GPa) was observed (Figure S3). On the basis of the unperturbed natural resonant mode of 32 071 Hz, a Young's modulus of 41.9 GPa was extracted from a linear fit to the data obtained from the simulation. This is in agreement with the reported averaged tensor value of 45 GPa.[37]

Measurements made over the full laser irradiance range (0.8−43 kW/cm^2, Figure 3c) show the eigenfrequency change as a function of laser irradiance. Eigenfrequencies appear to fall on an exponential decay curve (solid green line) which can be interpreted in the context of laser-induced heating (heating component) and optical-trapping stiffness (trapping component). The optical-trapping stiffness originates from a negative

DOI: 10.1021/acs.jpcc.8b00365
J. Phys. Chem. C 2018, 122, 7525−7532

pressure gradient force generated due to a tightly focused single beam of laser, which has been shown to trap particles from 25 nm to 10 μm.[20] At low irradiances, the linear red-shift in the eigenfrequency can be attributed to a decrease in the Young's modulus of the material as the cantilever heats up with an increase in laser irradiance (dashed red line). This corresponds to a rise in ΔT_{ms} (ΔT_{max}) of 371 K (1494 K) and a decrease of the Young's modulus to 40.03 GPa for a frequency red-shift of 701.2 Hz at a laser irradiance of 43 kW/cm^2. At high laser irradiances, the optical-trapping stiffness becomes significant and causes a decrease in the rate of the eigenfrequency's red-shift. The measured frequency at high irradiances is thus the net result of heating and laser-trapping components, shown using a dashed red line and a dotted blue line, respectively, in Figure 3c. The dotted blue line representing the laser-trapping stiffness experienced by the cantilever was obtained by subtracting the heating component (dashed red line) from the exponential fit (green line) and was further used to estimate its value at different laser irradiances using static structural simulation in COMSOL[27] (Figure S4a,b). The estimated trapping stiffness is shown in the right vertical axis in Figure 3c. It is important to note that although the radiation pressure force would cause a minimal deflection, it would not affect the eigenfrequency as no real mass is added to the system (see SI for details). Deconvolution of heating and trapping effects in the high laser irradiance range can be accomplished analytically by using a modified Euler–Bernoulli elastic beam model[38] for a uniform cross section cantilever modified with a spring attached at the tip of the cantilever (Figure S4a,b). The eigenfrequency (f_i) of the ith mode can be modeled according to the following equation:[39]

$$f_i = \frac{1}{2\pi}\frac{\Omega_i^2}{L^2}\sqrt{\left(\frac{EI}{\rho}\right)} \tag{1}$$

For a beam of length L and linear density ρ, E and I are the Young's modulus and area moment inertia of the cross section of the beam, respectively. The ith eigenvalue of nondimensional frequency coefficient Ω_i can be obtained by solving the eigenfunction for a given value of spring stiffness (K).[39]

$$-\left(\frac{K}{\Omega_i^3}\right)[\cos\Omega_i \sinh\Omega_i - \sin\Omega_i \cosh\Omega_i] + \cos\Omega_i \cosh\Omega_i + 1 = 0 \tag{2}$$

For a beam length, width, and height of 20 μm, 5 μm, and 110 nm, E = 45 GPa, and a density of 4826 kg/m^3, the calculated eigenfrequency of the first mode increases (blue-shifts) linearly from 7.0 to 70.3 Hz as the spring constant changes from 1 to 10 fN/nm (Figure S5), showing an increased blue-shift for a higher spring constant. As the analytical model is only valid for beams with uniform cross section, a finite element analysis was used to model the effects of a spring with stiffness (K) at the end of a cantilever geometry modeled on the basis of the sample dimensions to quantify the magnitude of optical-trapping stiffness observed experimentally.

The component of eigenfrequency that blue-shifts with increasing laser irradiance due to an increasing trapping force is shown as a dotted blue line in Figure 3c, indicating an increase in eigenfrequency with increasing irradiance, in the absence of heating. This was obtained by subtracting the heating component (dashed red line) from the exponential fit (green line). The resultant irradiance-dependent blue-shift was used to quantify the laser-trapping stiffness at high laser irradiances and is plotted in the right vertical axis of the plot (Figure 3c). Starting from a laser irradiance of 4.6 kW/cm^2, the laser-trapping stiffness is significant enough to affect the eigenfrequency and reaches a maximum of 9.1 fN/nm at 43 kW/cm^2 (Figure S4a,b). To better interpret the observed heating of the NR, an analysis of the heat transfer process was developed for the nanoribbon geometry shown in Figure 4a (see SI for details). Although the CdSNR shown in Figure 1b has a wedge shape, it can vary from a wedge shape to a ribbon with uniform cross section (WH) based on synthesis parameters discussed before.

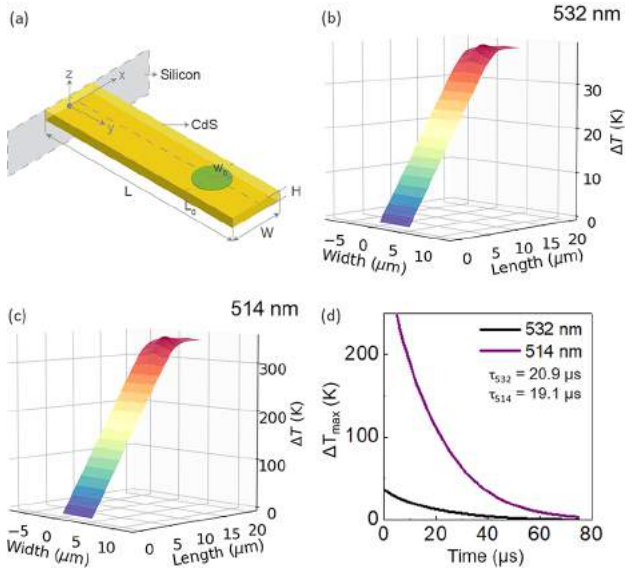

Figure 4. (a) CdS rectangular NR geometry used to derive the heat transfer theory, showing the x-, y-, and z-axes. The length (L), width (W), and height (H) have been labeled, and the position of the laser spot has been shown using a green circle of radius w_0, with center at $x = W/2$ and $y = L_0$. (b) The steady state surface temperature deviation from the ambient temperature (ΔT) of a CdS cantilever calculated for a thermal conductivity (κ) of 20 W/(m K), n = 2.5513 − i0.0057657, R_λ = 0.19081 (at 532 nm), laser spot radius w_0 = 1.15 μm, L = 20 μm, W = 5 μm, H = 110 nm, P_0 = 1.8 mW. (c) The ΔT profile of a CdS cantilever calculated for the same parameters as in part b, P_0 = 1.8 mW, and optical constants for 514 nm, n = 2.6399 − i0.055754 and R_λ = 0.20317 (at 514 nm). (d) The calculated cooling curve depicting the decay in the maximum steady state temperature (ΔT_{max}) with respect to time after the cantilever reached steady state temperatures and then the source was switched off. For comparison, the cooling curves calculated for the same geometry and respective optical constants for 532 and 514 nm are shown.

To examine the effects of heating by the laser beam we consider a CdS ribbon of length L, width W, and thickness H as shown in Figure 4a. It is convenient to write the energy equation for the electromagnetically heated ribbon in dimensionless form given by

$$\frac{\partial U}{\partial \tau} = a^2\frac{\partial^2 U}{\partial \xi^2} + \frac{\partial^2 U}{\partial \eta^2} + b^2\frac{\partial^2 U}{\partial \zeta^2} + \sigma \tag{3}$$

where the dimensionless parameters are defined by

DOI: 10.1021/acs.jpcc.8b00365
J. Phys. Chem. C 2018, 122, 7525−7532

Table 1. Summary of Results from Temperature Calculations Using Different Parameters in the Analytical Model[a]

L, W, H (μm)	λ_0 (nm)	reflectivity (R_λ)	refractive index (n)	P_0 (mW)	ΔT_{max} (K)	ΔT_{ms} (K)
20, 5, 0.11	532	0.19031	2.5513 − i0.005 7657	1.8	38.6	9.57
20, 5, 0.11	514	0.20317	2.6399 − i0.055 754	1.8	350	86.8
35, 2.3, 0.11	532	0.19031	2.5513 − i0.005 7657	0.1	6.69	1.66
35, 2.3, 0.11	532	0.19031	2.5513 − i0.005 7657	1.8	120	29.8
35, 2.3, 0.11	532	0.19031	2.5513 − i0.082 112	0.1	83	20.6 (20.6)
35, 2.3, 0.11	532	0.19031	2.5513 − i0.082 112	1.8	1494	371 (371)

[a]The experimentally measured values of ΔT_{ms} are shown in parentheses.

$$U = \frac{T - T_0}{T_0},\ \tau = \frac{\alpha t}{L^2},\ a = \frac{L}{W},\ b = \frac{L}{H},\ \xi = \frac{x}{W},\ \eta = \frac{y}{L},\ \zeta = \frac{z}{L},\ \sigma = \frac{L^2}{\kappa T_0}\dot{Q}''' \tag{4}$$

Here, $\alpha = \kappa/\rho C$ is the thermal diffusivity of the nanoribbon, T_0 is the temperature at its base ($y = 0$), and the approximation for the electromagnetic energy absorbed by the medium per unit volume per unit time at a radial distance of r from the center of the beam with a waist radius of w_0 and wavelength λ_0 *in vacuo* is given as

$$\dot{Q}'''(r, z) = \frac{4\pi n''}{\lambda_0} I_0(1 - R_\lambda)\exp\left(-\frac{2r^2}{w_0^2}\right)\exp(-2k''z) \tag{5}$$

where I_0 is the incident irradiance, R_λ is the wavelength-dependent reflectivity, n'' is the imaginary part of refractive index of the medium, and k'' is the corresponding wavenumber ($k'' = 2\pi n''/\lambda_0$).

Since the nanoribbon is mounted in a vacuum chamber, convective or conductive heat transfer from the suspended surfaces can be neglected. Furthermore, due to a small Biot number the radiant heat fluxes are extremely small for the temperatures and characteristic length scales involved here. Therefore, the boundary conditions are given by

$$\frac{\partial U}{\partial \xi}(0, \eta, \zeta, \tau) = \frac{\partial U}{\partial \xi}(1, \eta, \zeta, \tau) = \frac{\partial U}{\partial \zeta}(\xi, \eta, 0, \tau) = \frac{\partial U}{\partial \zeta}(\xi, \eta, 1, \tau) = 0 \tag{6}$$

and

$$U(\xi, 0, \zeta, \tau) = 0 \qquad \frac{\partial U}{\partial \eta}(\xi, 1, \zeta, \tau) = 0 \tag{7}$$

We look for a classical product solution of the form

$$U(\xi, \eta, \zeta, \tau) = \sum_{l=0}^{\infty}\sum_{m=0}^{\infty}\sum_{n=0}^{\infty} A_{lmn}(\tau)X_l(\xi)Y_m(\eta)Z_n(\zeta) \tag{8}$$

in which the orthonormal eigenfunctions $X_m(\xi)$ and $Y_n(\eta)$ satisfy homogeneous boundary conditions and are given by

$$X_l(\xi) = 1 \text{ for } l = 0 \text{ and } \sqrt{2}\cos(l\xi\pi) \text{ for } l = 1, 2, 3 \ldots \tag{9}$$

$$Y_m(\eta) = \sqrt{2}\sin\left(\left(m + \frac{1}{2}\right)\eta\pi\right) \text{ for } m = 0, 1, 2 \ldots \tag{10}$$

$$Z_n(\zeta) = 1 \text{ for } n = 0 \text{ and } \sqrt{2}\cos(n\zeta\pi) \text{ for } n = 1, 2, 3 \ldots \tag{11}$$

where prime indicates a dummy variable, and the coefficients of $A_{lmn}(\tau)$ are given by

$$A_{lmn}(\tau) = \frac{[1 - \exp(-\gamma_{lmn}^2\tau)]}{\gamma_{lmn}^2}\int_0^1\int_0^1\int_0^1 \sigma(\xi'\eta'\zeta')X_l(\xi')Y_m(\eta')Z_n(\zeta')d\xi' d\eta' d\zeta' \tag{12}$$

where

$$\gamma_{lmn}^2 = (al\pi)^2 + \left[\left(m + \frac{1}{2}\right)\pi\right]^2 + (bn\pi)^2 \tag{13}$$

The steady state solution is obtained by taking the limit as $\tau \to \infty$.

We note that σ vanishes outside of a region surrounding a cylinder with origin $x = W/2$, $y = L_0$ (or $\xi = 1/2$, $\eta = \eta^* = L_0/L$). We assume that the radius of that region is $W/2$, the half width of the nanoribbon. The double integral over the circular region can be obtained by quadrature using an appropriate numerical integration software (see SI for details).

Calculations were performed using the solution above with a thermal conductivity (κ) of 20 W/(m K), n = 2.5513 − i0.005 7657 and 2.6399 − i0.055 754 at 532 and 514 nm laser wavelengths, respectively, laser spot radius w_0 = 1.15 μm, L = 20 μm (spot center at 0.75 × L), W = 5 μm, H = 110 nm, P_0 = 1.8 mW; we predict a ΔT_{ms} (ΔT_{max}) of 9.7 K (38.6 K) and 87.5 K (350 K) for 532 and 514 nm incident lasers, respectively, indicating the importance of the imaginary refractive index (Figure 4b,c). In the calculations, a laser power of 1.8 mW was reduced to account for Fresnel reflection at normal incidence using R_λ values of 0.190 81 and 0.203 17 at 532 and 514 nm, respectively. A calculated steady state temperature deviation from the boundary temperature condition (ΔT) profile at the surface during irradiation with the 532 and 514 nm laser has been plotted in Figure 4b,c, respectively. Although the values on the temperature axis change, the general profile of the plot shown in Figure 4b,c remained the same for various laser powers.

For a rectangular geometry with L = 35 μm, W = 2.3 μm, H = 110 nm (similar to the NR used for eigenfrequency measurements) using the same optical constants mentioned above, and input 532 nm laser powers of 100 and 1800 μW, the ΔT_{ms} (ΔT_{max}) values were 6.69 K (1.66 K) and 120 K (29.8 K), respectively. Compared to the experimentally measured ΔT_{ms} (ΔT_{max}) of 20.6 K (82.7 K) at 100 μW, the analytical calculation underestimates the magnitude of the temperature rise. This deviation can be attributed to a variation in the value of the imaginary part of the refractive index probably due to impurities or nonstoichiometry of the CdSNR (Figure S6). A comparison between the experimentally observed and theoretically predicted temperature allows an estimation of the imaginary refractive index of the CdSNR. A ΔT_{ms} (ΔT_{max}) of

DOI: 10.1021/acs.jpcc.8b00365
J. Phys. Chem. C 2018, 122, 7525−7532

20.6 K (83 K) at 100 μW of laser power was obtained using an imaginary refractive index of 0.082 112 rather than that reported by Treharne et al.[40] (n'' = 0.005 7657). This estimated imaginary refractive index predicts a ΔT_{ms} (ΔT_{max}) of 371 K (1494 K) at 1800 μW, which is in agreement with the experimentally measured ΔT_{ms} (ΔT_{max}) of 371 K (1494 K) for the same laser power. Similar values of the steady state temperature obtained using the analytical model have been confirmed using finite element software (COMSOL[27]). The results of calculations using various parameters discussed have been summarized in Table 1. Values of w_0 = 1.15 μm and κ = 20 W/(m K) were used for all the tabulated calculations.

The transient heat transfer model from a finite element model for a cantilever beam irradiated by a 532 nm laser suggests time scales of 80 μs to reach within 0.1% of T_0 after the laser beam heat source is turned off. The ΔT_{max} versus time profiles have been plotted in Figure 4d. Similar time scales of 80 μs, independent of the laser power, were calculated for the time it takes to reach steady state after the laser source is turned on (Figure S7). These time scales (<100 μs) are significantly shorter than the minute-level time constants that have been reported in prior claims of CdSNR cooling.[5]

CONCLUSION

In summary, a novel optomechanical eigenfrequency measurement technique was developed for evaluating the temperature of the CdSNRs that have been reported to undergo laser cooling. Although the synthesized NRs were highly crystalline and exhibited a high yield of anti-Stokes PL, the eigenfrequencies were observed to decrease with increasing laser power due to heating at low laser powers and a possible laser-trapping force at higher laser powers. No evidence of laser cooling was observed. A rigorous discussion of a modified Euler−Bernoulli theory of a uniform cantilever with a spring attached to the free end in the context of high laser powers has been included to interpret the eigenfrequency data obtained. Theoretical simulations of photothermal heating using transient heat transfer analysis yield a maximum temperature rise and the time to attain steady state for various NR dimensions, laser powers, and optical constants. Combined with experimentally measured temperatures, the analytical model also allows the determination of the imaginary refractive index of the CdSNR. This approach is general and may be useful for measuring laser refrigeration in a range of different material systems.

ASSOCIATED CONTENT

Supporting Information

The Supporting Information is available free of charge on the ACS Publications website at DOI: 10.1021/acs.jpcc.8b00365.

Calculations of morphology-dependent resonances (Figure S1), finite-element eigenfrequency calculations (Figure S2), Young's-modulus-dependent eigenfrequency parametric sweep (Figure S3), laser radiation pressure calculations, laser-trap-stiffness-dependent frequency change calculations (Figures S4 and S5), calculation of the double quadrature for heat transfer analysis, energy-dispersive X-ray spectroscopy of CdSNRs (Figure S6 and Table S1), analytical solution for heat transfer analysis, time scales during laser heating (Figure S7), eigenfrequency measurements on CdSNRs from Zhang et al. (Figure S8 and Table S2), stability of eigenfrequency post irradiation (Figure S9), and coordinate-dependent Young's modulus (Figure S10, Table S3) (PDF)

AUTHOR INFORMATION

Corresponding Author

*E-mail: peterpz@uw.edu.

ORCID

Anupum Pant: 0000-0002-6253-8418

Matthew B. Lim: 0000-0001-6129-9876

Author Contributions

$^{\perp}$A.P. and B.E.S. contributed equally to this work.

Notes

The authors declare no competing financial interest.

ACKNOWLEDGMENTS

A.P. and P.J.P. gratefully acknowledge financial support from the MURI:MARBLe project under the auspices of the Air Force Office of Scientific Research (Award No. FA9550-16-1-0362). M.J.C. gratefully acknowledges support from the DOD through National Defense Science and Engineering Graduate Research (NDSEG) Fellowship. Finally, we thank Mansoor Sheik-Bahae, Jacob Khurgin, Masaru Kuno, and Qihua Xiong for fruitful discussions during the course of this work and Qihua Xiong's lab for sending their cadmium sulfide nanoribbon samples. AFM and TEM were conducted at the University of Washington Molecular Analysis Facility, which is supported in part by the National Science Foundation (Grant No. ECC-1542101), the University of Washington, the Molecular Engineering & Sciences Institute, the Clean Energy Institute, and the National Institutes of Health.

REFERENCES

(1) Agarwal, R.; Barrelet, C. J.; Lieber, C. M. Lasing in Single Cadmium Sulfide Nanowire Optical Cavities. *Nano Lett.* **2005**, *5*, 917−920.

(2) Liu, B.; Chen, R.; Xu, X.; Li, D.; Zhao, Y.; Shen, Z.; Xiong, Q.; Sun, H. Exciton-Related Photoluminescence and Lasing in CdS nanobelts. *J. Phys. Chem. C* **2011**, *115*, 12826−12830.

(3) Nasalevich, M. A.; Kozlova, E. A.; Lyubina, T. P.; Vorontsov, A. V. Photocatalytic Oxidation of Ethanol and Isopropanol Vapors on Cadmium Sulfide. *J. Catal.* **2012**, *287*, 138−148.

(4) Peng, T.; Li, K.; Zeng, P.; Zhang, Q.; Zhang, X. Enhanced Photocatalytic Hydrogen Production Over Graphene Oxide−Cadmium Sulfide Nanocomposite Under Visible Light Irradiation. *J. Phys. Chem. C* **2012**, *116*, 22720−22726.

(5) Zhang, J.; Li, D.; Chen, R.; Xiong, Q. Laser Cooling of a Semiconductor by 40 K. *Nature* **2013**, *493*, 504−508.

(6) Thomas, D.; Hopfield, J. Exciton Spectrum of Cadmium Sulfide. *Phys. Rev.* **1959**, *116*, 573−582.

(7) Fröhlich, H. Interaction of Electrons with Lattice Vibrations. *Proc. R. Soc. London, Ser. A* **1952**, *215*, 291−298.

(8) Sheik-Bahae, M.; Epstein, R. I. Optical Refrigeration. *Nat. Photonics* **2007**, *1*, 693−699.

(9) Lemos, A. M. Huang-Rhys Factors for Absorption and Emission of Light by F-Centers. Ph.D. Thesis, Illinois Institute of Technology, Chicago, IL, 1964.

(10) Li, D.; Zhang, J.; Xiong, Q. Laser Cooling of CdS Nanobelts: Thickness Matters. *Opt. Express* **2013**, *21*, 19302−19310.

(11) Seletskiy, D. V.; Melgaard, S. D.; Epstein, R. I.; Di Lieto, A.; Tonelli, M.; Sheik-Bahae, M. Precise Determination of Minimum Achievable Temperature for Solid-State Optical Refrigeration. *J. Lumin.* **2013**, *133*, 5−9.

DOI: 10.1021/acs.jpcc.8b00365
J. Phys. Chem. C 2018, 122, 7525−7532

(12) Roder, P. B.; Smith, B. E.; Zhou, X.; Crane, M. J.; Pauzauskie, P. J. Laser Refrigeration of Hydrothermal Nanocrystals in Physiological Media. *Proc. Natl. Acad. Sci. U. S. A.* **2015**, *112*, 15024−15029.
(13) McLaurin, E. J.; Bradshaw, L. R.; Gamelin, D. R. Dual-Emitting Nanoscale Temperature Sensors. *Chem. Mater.* **2013**, *25*, 1283−1292.
(14) Dong, B.; Hua, R. N.; Cao, B. S.; Li, Z. P.; He, Y. Y.; Zhang, Z. Y.; Wolfbeis, O. S. Size Dependence of the Upconverted Luminescence of NaYF:4 Er, Yb Microspheres for Use in Ratiometric Thermometry. *Phys. Chem. Chem. Phys.* **2014**, *16*, 20009−20012.
(15) Seletskiy, D. V.; Hasselbeck, M. P.; Sheik-Bahae, M.; Epstein, R. I. Fast Differential Luminescence Thermometry. *Proc. SPIE 7228, Laser Refrigeration of Solids II*; San Jose, CA, Feb 10, 2009; p 72280K.
(16) Ha, S.-T.; Shen, C.; Zhang, J.; Xiong, Q. Laser Cooling of Organic-Inorganic Lead Halide Perovskites. *Nat. Photonics* **2016**, *10*, 115−121.
(17) Manzke, G.; Peng, Q.; Henneberger, K.; Neukirch, U.; Hauke, K.; Wundke, K.; Gutowski, J.; Hommel, D. Density Dependence of the Exciton Energy in Semiconductors. *Phys. Rev. Lett.* **1998**, *80*, 4943−4976.
(18) Hartland, G. V.; Hu, M.; Sader, J. E. Softening of the Symmetric Breathing Mode in Gold Particles by Laser-Induced Heating. *J. Phys. Chem. B* **2003**, *107*, 7472−7478.
(19) Major, T. A.; Lo, S. S.; Yu, K.; Hartland, G. V. Time-Resolved Studies of the Acoustic Vibrational Modes of Metal and Semiconductor nano-objects. *J. Phys. Chem. Lett.* **2014**, *5*, 866−874.
(20) Ashkin, A.; Dziedzic, J. M.; Bjorkholm, J.; Chu, S. Observation of a Single-Beam Gradient Force Optical Trap for Dielectric Particles. *Opt. Lett.* **1986**, *11*, 288−290.
(21) Li, H.; Chen, L.; Zhao, Y.; Liu, X.; Guan, L.; Sun, J.; Wu, J.; Xu, N. Effects of Experimental Conditions on the Morphologies, Structures and Growth Modes of Pulsed Laser-Deposited CdS Nanoneedles. *Nanoscale Res. Lett.* **2014**, *9*, 91.
(22) Gao, T.; Wang, T. Two-Dimensional Single Crystal CdS Nanosheets: Synthesis and Properties. *Cryst. Growth Des.* **2010**, *10*, 4995−5000.
(23) Crane, M. J.; Pauzauskie, P. J. Mass Transport in Nanowire Synthesis: An Overview of Scalable Nanomanufacturing. *J. Mater. Sci. Technol.* **2015**, *31*, 523−532.
(24) Wang, C.; Li, C.-Y.; Hasselbeck, M. P.; Imangholi, B.; Sheik-Bahae, M. Precision, All-Optical Measurement of External Quantum Efficiency in Semiconductors. *J. Appl. Phys.* **2011**, *109*, 093108.
(25) Lee, J.; Goericke, F.; King, W. P. Temperature-Dependent Thermomechanical Noise Spectra of Doped Silicon Microcantilevers. *Sens. Actuators, A* **2008**, *145*, 37−43.
(26) Pini, V.; Tamayo, J.; Gil-Santos, E.; Ramos, D.; Kosaka, P.; Tong, H.-D.; van Rijn, C.; Calleja, M. Shedding Light on Axial Stress Effect on Resonance Frequencies of Nanocantilevers. *ACS Nano* **2011**, *5*, 4269−4275.
(27) *Comsol*, version 4.2; COMSOL Inc.: Burlington, MA, 2011.
(28) Jin, L.; Wang, J.; Jia, S.; Sang, H.; Deng, L.; Yan, X.; Cai, Y.; Lu, P.; Choy, W. C. Twinning Mediated Growth of ZnSe Tri and Bi-crystal Nanobelts with Single Crystalline Wurtzite Nanobelts as Building Blocks. *CrystEngComm* **2010**, *12*, 150−158.
(29) Morozov, Y. V.; Draguta, S.; Zhang, S.; Cadranel, A.; Wang, Y.; Janko, B.; Kuno, M. Defect-Mediated CdS Nanobelt Photoluminescence Up-Conversion. *J. Phys. Chem. C* **2017**, *121*, 16607−16616.
(30) Tell, B.; Damen, T.; Porto, S. Raman Effect in Cadmium Sulfide. *Phys. Rev.* **1966**, *144*, 771−774.
(31) Hu, C.; Zeng, X.; Cui, J.; Chen, H.; Lu, J. Size Effects of Raman and Photoluminescence Spectra of CdS Nanobelts. *J. Phys. Chem. C* **2013**, *117*, 20998−21005.
(32) Phuruangrat, A.; Thongtem, T.; Thongtem, S. Characterization and Photonic Absorption of Hierarchical Tree-Like CdS Nanostructure Synthesized by Solvothermal Method. *Mater. Lett.* **2012**, *80*, 114−116.
(33) Chuu, D.; Dai, C.; Hsieh, W.; Tsai, C. Raman Investigations of the Surface Modes of the Crystallites in CdS Thin Films Grown by Pulsed Laser and Thermal Evaporation. *J. Appl. Phys.* **1991**, *69*, 8402−8404.
(34) Abdulkhadar, M.; Thomas, B. Study of Raman Spectra of Nanoparticles of CdS and ZnS. *Nanostruct. Mater.* **1995**, *5*, 289−298.
(35) Johnson, B. Theory of Morphology-Dependent Resonances: Shape Resonances and Width Formulas. *J. Opt. Soc. Am. A* **1993**, *10*, 343−352.
(36) Roder, P. B.; Pauzauskie, P. J.; Davis, E. J. Nanowire Heating by Optical Electromagnetic Irradiation. *Langmuir* **2012**, *28*, 16177−16185.
(37) Gerlich, D. The Elastic Constants of Cadmium Sulfide Between 4.2−300° K. *J. Phys. Chem. Solids* **1967**, *28*, 2575−2579.
(38) Bauchau, O.; Craig, J. *Structural Analysis*; Springer: Dordrecht, Netherlands, 2009; pp 173−221.
(39) Balachandran, B.; Magrab, E. B. *Vibrations*; Cengage Learning: Toronto, Canada, 2008; pp 23−68.
(40) Treharne, R.; Seymour-Pierce, A.; Durose, K.; Hutchings, K.; Roncallo, S.; Lane, D. Optical Design and Fabrication of Fully Sputtered CdTe/CdS Solar Cells. *J. Phys. Conf. Ser.* **2011**, *286*, 012038.

DOI: 10.1021/acs.jpcc.8b00365
J. Phys. Chem. C 2018, 122, 7525−7532